NANO LETTERS
Letter
Cite This: Nano Lett. 2018, 18, 7942−7948
pubs.acs.org/NanoLett

High Performance Plasmonic Nanolasers with External Quantum Efficiency Exceeding 10%

Suo Wang,[†] Hua-Zhou Chen,[†] and Ren-Min Ma*[,†,‡]

[†]State Key Lab for Mesoscopic Physics and School of Physics, Peking University, Beijing 100871, China
[‡]Collaborative Innovation Center of Quantum Matter, Beijing 100871, China

Supporting Information

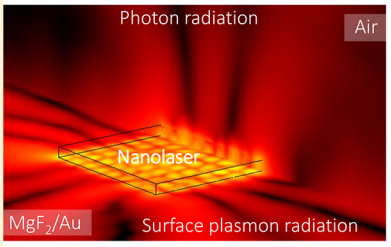

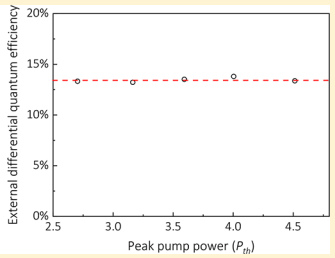

ABSTRACT: Plasmonic nanolasers break the diffraction limit for an optical oscillator, which brings new capabilities for various applications ranging from on-chip optical interconnector to biomedical sensing and imaging. However, the inevitably accompanied metallic absorption loss could convert the input power to heat rather than radiations, leading to undesired low external quantum efficiency and device degradation. To date, direct characterization of quantum efficiency of plasmonic nanolasers is still a forbidden task due to its near-field surface plasmon emissions, divergent emission profile, and the limited emission power. Here, we develop a method to characterize the external quantum efficiency of plasmonic nanolasers by synergizing experimental measurement and theoretical calculation. With systematical device optimization, we demonstrate high performance plasmonic nanolasers with external quantum efficiency exceeding 10% at room temperature. This work fills in a missing yet essential piece of key metrics of plasmonic nanolasers. The demonstrated high external quantum efficiency of plasmonic nanolasers not only clarifies the long-standing debate, but also endorses the exploration of them in various practical applications such as near-field spectroscopy and sensing, integrated optical interconnects, solid-state lighting, and free-space optical communication.

KEYWORDS: *Plasmonic nanolaser, spasers, quantum efficiency, semiconductor lasers*

Plasmonic nanolasers are a new class of laser devices with strong field confinement beyond the diffraction limit of light. They offer simultaneous light field localization in frequency, time, and space and are an emergent tool for many applications, ranging from on-chip optical interconnector to biomedical sensing and imaging.[1−6] To date, great progress has been made in materials research and development of proof-of-concept devices in numerous configurations including metallic-coated nanolaser,[7−15] plasmonic nanowire laser,[16−28] metal−insulator−metal gap mode nanolaser,[29] metallic-nanoparticle laser,[30−33] nanopatch laser,[34] nanodisk laser,[35] nanosquare laser,[36−42] plasmonic crystal nanolaser,[43−45] coaxial nanolaser,[46,47] waveguide embedded plasmonic nanolaser,[48] pseudowedge nanolaser,[49] hyperbolic metacavity laser,[50] metallic particle array laser, etc.[51−57] Most recently, plasmonic nanolasers have been exploited in a variety of applications including integrated photonic circuits, sensing, and biological probe.[33,37,38,41,45,48] However, the main power consumed by a plasmonic nanolaser could be converted to heat by the intrinsic metallic absorption rather than radiations, leading to undesired low external quantum efficiency and device degradation due to thermal effect. Despite the rapidly advanced research in plasmonic nanolasers, the external quantum efficiency, one of the most important laser key metrics, of plasmonic nanolasers remains unrevealed, which shakes the foundation of exploring them in various practical applications.

The loss of a laser device consists of material loss and radiation loss. While the total loss determines the threshold and the power consumption of a laser, it is the material loss that determines the external quantum efficiency (EQE). EQE characterizes not only the emission power for practical utility, but also how much power is converted to heat that degrades the laser performance. In conventional semiconductor lasers, the material loss originates from the stimulated absorption and nonradiative recombination. While the nonradiative recombination can be mediated by materials optimization, the stimulated absorption is rather intrinsic: to reach a net gain for amplification, the gain materials have to be pumped over a transparency state to achieve population inversion.

Received: September 26, 2018
Revised: November 10, 2018
Published: November 13, 2018

DOI: 10.1021/acs.nanolett.8b03890
Nano Lett. 2018, 18, 7942−7948

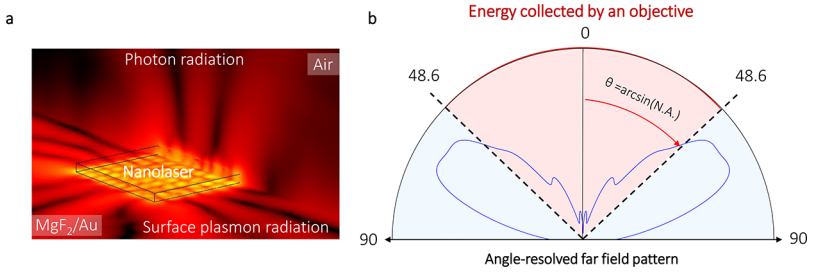

Figure 1. Radiations field of plasmonic nanolasers. (a) Typical three-dimensional radiation pattern of a square shaped plasmonic nanolaser obtained via three-dimensional full wave simulation. The radiation field of plasmonic nanolasers consists two parts, the photons scattered to the optical far field and the dark emission of surface plasmons propagating evanescently in the near field. (b) Angle-resolved far field pattern of a square shaped plasmonic nanolaser. The pink fan area indicates the part that is collected by an objective with a numerical aperture of 0.75.

The introduction of plasmonic confinement in a laser cavity can lower the total cavity loss by significantly suppressing the radiation loss.[42] However, it inevitably brings another material loss channel of free carrier absorptions in metal. In a plasmonic nanolaser cavity, the metallic loss can be dominant over the radiation loss and the gain material loss, leading to undesired low external quantum efficiency and device degradation, which provokes a long-standing debate over the viability of metal confinement and feedback strategies in laser technology.

Notwithstanding the fast development of the research in plasmonic nanolasers, to date, direct characterization of quantum efficiency of plasmonic nanolasers is still a forbidden task. First, a significant of output power of plasmonic nanolasers is in the form of surface plasmon polaritons, which is a dark emission not radiating to free space. Second, the strong beam divergence due to the field confinement prevents efficient output power collection. Last, the low output power due to the limited gain volume challenges the direct measurement using normal quantum efficiency characterization tool such as integrating sphere.

Here, for the first time, we quantitatively characterize the external quantum efficiency of plasmonic nanolasers by synergizing experimental measurement and theoretical calculation. We demonstrate that the external quantum efficiency of a plasmonic nanolaser can exceed 10% with that the optical mode is confined in a deep-subwavelength scale of 0.048 λ^3 where λ is the lasing emission wavelength of 700 nm. Furthermore, other key metrics of the demonstrated plasmonic nanolaser are also with high performance, which include a record narrow emission line width of 0.28 nm and a low threshold power consumption of 3.5 mW at room temperature. The demonstrated high performance plasmonic nanolaser with external quantum efficiency exceeding 10% clarifies the long-standing debate and will endorse the exploration of them in various practical applications.

Results. *External Quantum Efficiency of Plasmonic Nanolasers.* In contrast to conventional lasers, the radiation field of plasmonic nanolasers consists of two parts, the photons scattered to the optical far field and the dark emission of surface plasmons propagating evanescently in the near field.[28,40] Consequently, the EQE of plasmonic nanolasers should contain both of these emission powers and thereby can be defined as $\eta_{EQE} = \frac{(P_{photon} + P_{SPP}) / h\nu}{P_{IN} / h\nu_{IN}}$, where P_{IN} and $h\nu_{IN}$ are the pump power and pump photon energy, respectively, P_{photon} and P_{SPP} are the emitted powers of photons and surface plasmons, respectively, and $h\nu$ is the energy of the emitted phonons and surface plasmons.

Figure 1a shows a typical three-dimensional radiation pattern of a square shaped plasmonic nanolaser obtained via three-dimensional full wave simulation. Conventional EQE characterization methods can be hardly employed here to measure the power of the emission: the small cavity size results in a limited photon emission power with strong divergence, which can be hardly measured by either a power meter or an integrating sphere. The intrinsic surface plasmon emission propagating along the metal-dielectric interface puts another hurdle for the direct measurement of the emission power because it only exists in the near field due to the momentum mismatch with optical fields in the free space.[48]

To characterize the EQE of plasmonic nanolasers, we here utilized a fundamental feature of the laser emission field of that any lasing mode must be an eigenmode of the laser cavity. For a nanoscale laser, only a limited number of eigenmodes exist in the cavity with spectral overlap with gain spectrum, which gives the feasibility to identify the lasing eigenmodes. Especially for a single mode laser, we can reveal the full lasing properties providing the lasing eigenmode is identified and reconstructed by three-dimensional full wave simulation. Thereby, we can extrapolate the full emission power by only measure a certain part of it (Figure 1b).

External Quantum Efficiency Optimization. A high EQE of plasmonic nanolasers requires both high internal quantum efficiency of its gain material and high extraction efficiency of its cavity, representing the dynamics of photon generation and radiation processes, respectively. While the internal quantum efficiency reflects the competition between the radiative and nonradiative recombination rate of the excited electron−hole pairs, the extraction efficiency reflects the competition between the radiation and metallic dissipation rate of the cavity. We note that both the dynamics of photon generation and radiation processes will be affected by the small cavity size of a plasmonic nanolaser.

For the internal quantum efficiency optimization, high quality gain materials with suppressed nonradiative recombination are crucial. Here we employ high quality single crystalline CdSe nanosquares with smooth surfaces and high crystal quality as the gain material (see Supporting Information section 1). The dynamics of photon generation process of CdSe will be altered after the construction of the plasmonic nanolaser cavity: because of the strong spatial and spectral localization of nanocavity modes, the radiation recombination rate is accelerated by the Purcell effect, which suppresses the nonradiative recombination and improves the internal quantum efficiency close to unity.[42]

DOI: 10.1021/acs.nanolett.8b03890
Nano Lett. 2018, 18, 7942−7948

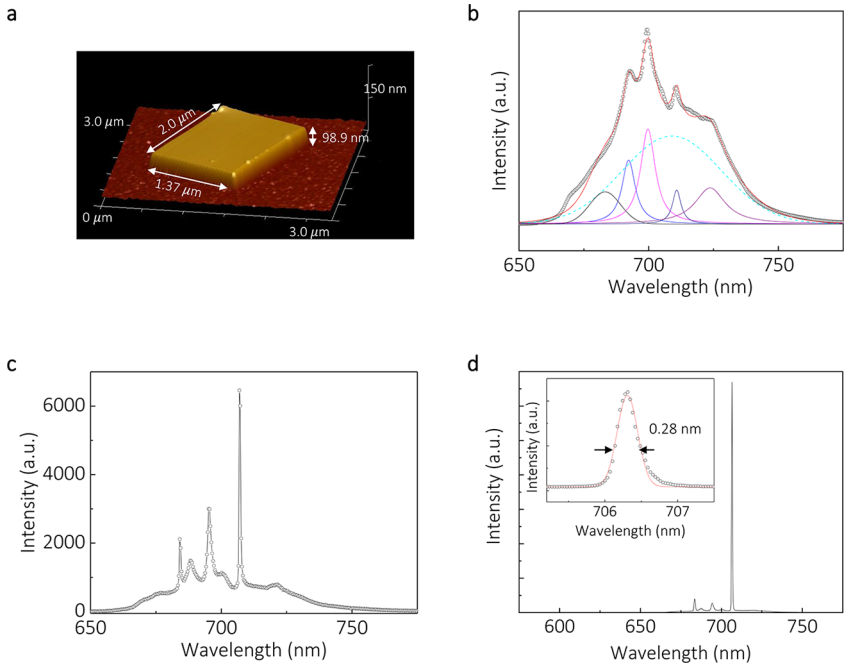

Figure 2. Morphology and spectra of a CdSe nanosquare plasmonic nanolaser. (a) Morphology of a plasmonic nanolaser where CdSe nanosquare with a size of 98.9 nm × 2.0 μm × 1.37 μm. (b) Spontaneous emission spectrum of the device pumped at a peak pump power of ∼2.5 mW. There are five pronounced cavity modes appearing as fringes in the spectrum with a broad spontaneous emission background indicated by the dashed curve. (c) Spectrum of the device pumped at a peak pump power of 1.7 P_{th}. With the increased pump power, the line widths and intensities of these cavity modes become narrower and stronger. (d) Spectrum of the device pumped at a peak pump power of 3.6 P_{th}, single mode lasing behavior is observed with a line width of 0.28 nm.

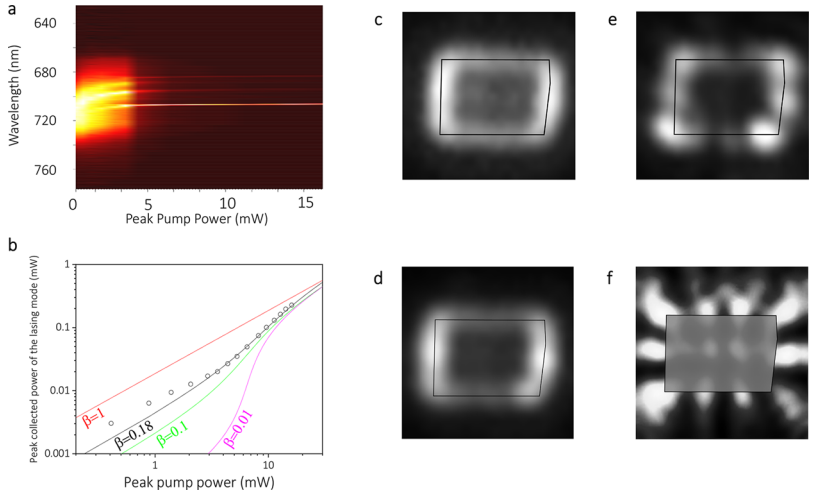

Figure 3. Spontaneous emission to stimulated emission phase transition in spectrum, intensity, and emission pattern. (a) Normalized emission spectra versus peak pump power, showing a clear transition from cavity mode modified spontaneous emissions to lasing emissions. (b) Light−light curve of the lasing mode of the plasmonic nanolaser. The spontaneous emission coupling factor (β factor) of the lasing cavity mode is obtained to be about 0.18 from a fitting of the light−light curve using rate equation. (c−e) Images of the plasmonic nanolaser when the pump power is (c) below threshold, (d) around threshold, and (e) above threshold. When below threshold (∼0.3 P_{th}), the emission pattern is the superposition of the multiple modes and appears uniformly around the cavity edge. Around threshold (∼1.7 P_{th}), discrete beams become to appear in the emission pattern. Above threshold (∼3.6 P_{th}), stimulated emission directs more photons to the single lasing mode, leading to the single mode operation and therefore making the pattern of the lasing mode more pronounced over other cavity modes. (f) Near field |**E**| field distribution of the lasing mode simulated by three-dimensional full wave simulation.

To have a high extraction efficiency, we have optimized the gold thin film in the plasmonic nanolaser cavity being polycrystalline structure with grain size larger than 50 nm and a high figure of merit, $\frac{-Re[\varepsilon_m]}{Im[\varepsilon_m]}$, of 16, where ε_m is the complex permittivity of gold[42] (see Supporting Information section 2). Theoretically, extraction efficiency can be calculated by $\frac{Q_{metal}}{Q_{metal}+Q_{rad}}$, where Q_{metal} and Q_{rad} are the absorption quality factor limited by metallic loss and radiation quality factor of a plasmonic nanocavity, respectively. We note that although a cavity with low radiation quality factor will increase its external quantum efficiency, it will degrade the performance of the

DOI: 10.1021/acs.nanolett.8b03890
Nano Lett. 2018, 18, 7942−7948

cavity by increasing the laser threshold and broadening the lasing emission line width.[48] Here, we have optimized the absorption and the radiation quality factor simultaneously to have an overall high performance by employing total internal reflection mode in a nanosquare cavity with smooth surfaces.

High Performance Plasmonic Nanolaser. Figure 2a shows the morphology of a plasmonic nanolaser where CdSe nanosquare with a size of 98.9 nm × 2.0 μm × 1.37 μm serves as gain material. With the strong plasmonic field confinement, the mode volume of the device is only about 0.048 λ^3, much smaller than its physical volume. We pumped the device by a nanosecond laser with a pulse width of 5 ns and a repetition rate of 12 kHz. Figure 2b shows the spontaneous emission spectrum of the device pumped at a peak pump power of ∼2.5 mW (∼0.7 P_{th}, where P_{th} = 3.5 mW is the peak pump power at lasing threshold). There are five pronounced cavity modes appearing as fringes in the spectrum (see Supporting Information section 3) and a broad spontaneous emission background. The mode centered at 710 nm is with the highest quality factor of 178. We note that cavity modified spontaneous emissions are usually observed in cavities with high quality factor such as photonic crystals and dielectric microdisc cavities where there is limited radiation and material losses. In plasmonic laser cavities, they were rarely observed.[36] Such pronounced cavity mode fringes not only indicate that our plasmonic cavity is with a high quality factor, but also show the emission of the gain material is efficiently coupled to the cavity modes.

The high quality of the cavity has a direct impact on the lasing performance. With the increased pump power (∼1.7 P_{th}), the line widths and intensities of these cavity modes become narrower and stronger (Figure 2c). When the device is pumped at a peak input power of 12.7 mW (∼3.6 P_{th}), single mode lasing behavior is observed with a line width of 0.28 nm (Figure 2d), which is, to our knowledge, a record value among all the reported plasmonic nanolasers. The single mode lasing with a side mode suppression ratio of 12 dB leads to an emission pattern distinct to that of the spontaneous emission one as discussed below.

Figure 3a shows the normalized emission spectra versus peak pump power, where we can see a clear transition from cavity mode modified spontaneous emissions to lasing emissions. The blue shift of the resonant cavity modes is due to the increased carrier concentration with the increased pump intensity, which saturates above the laser threshold due to the gain clamping. The strong coupled gain and cavity is also shown in light−light curve. As shown in Figure 3b, the light−light curve of the lasing cavity mode is in an "S" shape in log−log scale, identifying the phase transition from spontaneous to stimulated emission (the light−light curve of integrated power from all modes is shown in Supporting Information section 4). The transition can also be verified by line width narrowing of the lasing cavity mode as pump power increases (see Supporting Information section 5). The spontaneous emission coupling factor (β factor) of the device is obtained to be about 0.18 from a fitting of the light−light curve of the lasing cavity mode using rate equation.

Any lasing mode has to be an eigenmode of a laser cavity. Consequently, a cavity defined emission pattern supplies an important evidence for verifying lasing behavior and can be used to identify the exact lasing eigenmode.[28,40] Figure 3c shows the spontaneous emission image below threshold. It is the superposition of the multiple cavity modes, and because of that, the emission appears uniformly around the cavity edge. Around threshold, discrete beams begin to appear in the emission patterns (Figure 3d). Above threshold, stimulated emission directs more photons to the lasing mode, leading to the single mode operation and therefore making the pattern of the lasing mode more pronounced over other cavity modes (Figure 3e). In the lasing regime, the emission pattern remains unchanged under varied pump power (see Supporting Information section 6). We have used three-dimensional full wave simulation to identify the lasing mode. The simulated near field |**E**| field distribution of the lasing mode is shown in the Figure 3f, which shares the same main feature with the experimental pattern (see Supporting Information section 7). The simulated near field |**E**| distribution also remains unchanged under various gain (see Supporting Information section 8). All the emission features of the lasing mode can be extracted from the simulation.

Determining External Quantum Efficiency. In the following, we discuss the method to determine the input and output power of the plasmonic nanolaser for EQE calculation. For the input power of the device, we develop a method to determine it via measuring the reflected power of the pump laser beam. In the experiment, we first measure the absolute reflected power of the pump laser beam at the Au/air interface and then move the pump beam onto a CdSe nanosquare to get the absolute reflected power of the pump laser beam with the device being excited (see Supporting Information section 9). Because of the absorption of the CdSe nanosquare, the power of the reflected pump laser beam will decrease. Such a contrast P_{con} between the absolute power reflected at the Au/air interface and device interface approximately equals to the input power absorbed by CdSe gain materials. To obtain a more precise value, we further consider the reflectivity of each material interface and the absorptions of both Au and CdSe (see Methods). After these calibrations, the absolute absorption power of the device should be ∼1.10 P_{con} (see Supporting Information section 10). Note that edges and corners of the nanocavity will result in scattering that cannot be collected by the objective due to the limited numerical aperture. Thereby, the EQE can be underestimated here due to the overestimation of the input pump power.

For the output power, notably, the value we obtained in Figure 3e is the absolute far field emission power that is collected by the objective. At a pump power of 12.7 mW (∼3.6 P_{th}), the collection efficiency (the ratio between objective collected power and pump power) by the objective is 2.0%. To obtain the ratio of the collected power over total far field radiation power, we have calculated the far field emission pattern of the nanolaser from the near field pattern using the Stratton-Chu formula.[58] Considering the nanolaser being placed in the vicinity of the origin, the electric field at far field point p defined by an angular position (θ, ϕ) can be calculated by

$$\boldsymbol{E}_p = \frac{ik}{4\pi}\boldsymbol{r}_0 \times \int [\boldsymbol{n} \times \boldsymbol{E} - \eta \boldsymbol{r}_0 \times (\boldsymbol{n} \times \boldsymbol{H})]\, e^{ik\boldsymbol{r}\cdot\boldsymbol{r}_0}\, dS \quad (1)$$

where $\boldsymbol{E}$ and $\boldsymbol{H}$ are near field electric and magnetic fields of the lasing cavity eigenmode on the "aperture", the surface S enclosing the device, $\boldsymbol{r}$ is the radius vector on the surface S, $\boldsymbol{n}$ is the unit normal to the surface, η is the wave impedance in vacuum, k is the wavenumber corresponding to the frequency of the eigenmode, and $\boldsymbol{r}_0$ is the unit vector pointing from the

DOI: 10.1021/acs.nanolett.8b03890
Nano Lett. 2018, 18, 7942−7948

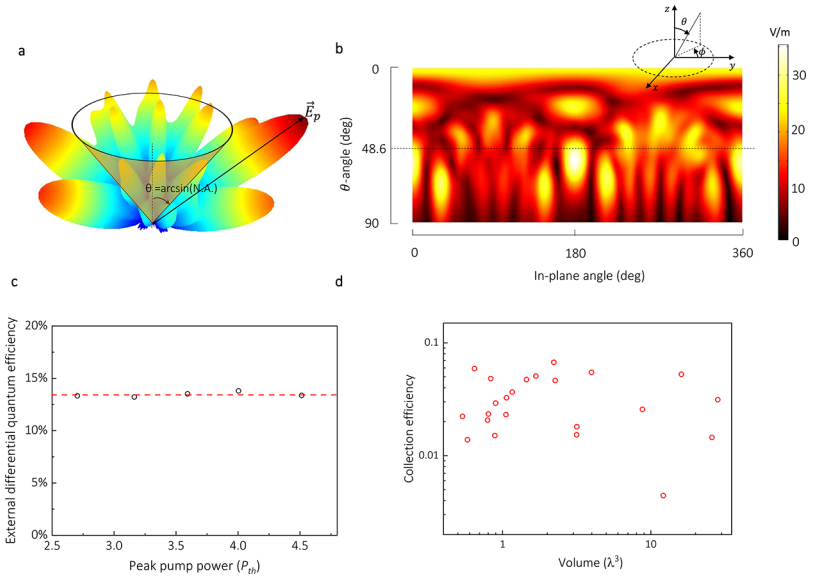

Figure 4. Determining the external quantum efficiency of plasmonic nanolaser. (a) Calculated far field radiation pattern of the lasing cavity mode. The ratio of the energy collected by the objective to the total energy radiated to the free space is about 38.2%. (b) Angle-resolved field distribution of the lasing cavity mode. Radiation with θ<48.6° (beneath the black dotted line) can be collected by the lens. (c) External differential quantum efficiency versus peak pump power above the lasing threshold. (d) Collection efficiency of plamonic nanolasers with varied physical volume. λ is the emission wavelength of 700 nm.

origin to the field point p, which is taken at infinity but with a well-defined angular position (θ, ϕ).

Figure 4 shows the calculated far field radiation pattern of the lasing cavity mode. Because the power flow of the far field is proportion to $|\mathbf{E}_p|^2$, the ratio of the power collected by the objective to the total power radiated to the free space can then be calculated from the far field radiation pattern, which is to be about 38.2%. The peak emission power of this directly collected radiation is about 0.26 mW. Thereby, we can get the full radiated photon power to be about 0.68 mW. We further calculate the ratio of the total far field radiation over the total radiation power from the full wave simulated lasing eigenmode, which is 60%. Then we get the total radiation power of the plasmonic nanolaser to be 1.13 mW, which corresponds to an external quantum efficiency, η_{EQE} of 11.9% (at 3.6 P_{th}). Figure 4c shows the external differential quantum efficiency versus peak pump power above the lasing threshold. The external differential quantum efficiency is about 13.4% in the measured pump power range.

We have measured more than 20 plasmonic nanolasers with various physical size as shown in Figure 4d. There is a general trend that smaller device has a higher collection efficiency. Such a trend is because that a smaller cavity has a lower radiation quality factor and thus a higher extraction efficiency.

The high EQE of the plasmonic nanolaser secures a high enough emission power for its practical application. For instance, in integrated optical interconnects, there is a lower bound of the emission power for its driving laser set by the sensitivity of the optical receiver in optical interconnects. The photon number in a bit needs to be larger than ~1000 for an error free data communication (bit error rate equaling to 10^{-12}) due to the thermal noise. At a bit rate of 10 Gb/s, it requires the laser emission power to be over 2.8 μW (at 700 nm here). We can see that the emission power of the plasmonic nanolaser reported here satisfies such a requirement.

Discussion. While a plasmonic nanolaser with small physical volume of gain material can lower the overall power consumption, its feasibility in many applications replies on its performance in EQE. A high EQE not only secures enough output power, but also avoids severe device degradation due to thermal effect. In this work, we develop a method to characterize the EQE of a plasmonic nanolasers and demonstrate that it can exceed 10% at room temperature. The constructed plasmonic nanolaser is also with high performance in other laser key metrics including a record narrow emission line width of 0.28 nm and a lower power consumption of 3.5 mW. Our work solves the challenges in characterizing the last yet essential key metric of plasmonic nanolasers. The demonstrated high EQE will endorse the exploration of them in various practical applications. We note that the EQE of plasmonic nanolasers can be further increased by accelerating their radiation rate via employing a smaller cavity with lower radiation quality factor, where cavity configuration engineering, metal quality improvements are crucial for loss compensation by gain materials. A higher EQE can also be realized by coupling a plasmonic nanolaser to an embedded waveguide, where not only the radiation efficiency can be enhanced, but also the emission directionality can be recovered.[48]

Methods. *Material Growth.* The gain material of CdSe is synthesized via a chemical vapor deposition method. CdSe powders with a purity of 99.99% were used as the source. A 10 nm thick Au film coated on silicon substrate was used as catalyst, which was deposited by thermal evaporation. During the growth process, high-purity argon was used as the carrier gas with a flow-rate of 100 standard-state cubic centimeter per minute. The temperature and duration were set to be 700 °C and 0.5 h.

Device Fabrication. The as fabricated CdSe nanosquares by chemical vapor deposition method were dry transferred to substrates of MgF_2/Au (5 nm/200 nm) to form plasmonic nanocavities. The plasmonic substrates was deposited by electron-beam evaporation, where the grain size of the Au polycrystalline film is larger than 50 nm. Under optical

DOI: 10.1021/acs.nanolett.8b03890
Nano Lett. 2018, 18, 7942−7948

pumping, CdSe nanosquares supply optical gain as well as the feedback cavity for a plasmnonic lasing behavior.

Mode Volume Calculation. The optical mode volume of plasmonic nanolaser cavities is calculated by $V_{mode} = \frac{\int \frac{1}{2}\left[Re\left[\frac{d(\omega\varepsilon)}{d\omega}\right]|\boldsymbol{E}(\boldsymbol{r})|^2 + \mu|\boldsymbol{H}(\boldsymbol{r})|^2\right] d^3\boldsymbol{r}}{\max\left[\frac{1}{2}\left[Re\left[\frac{d(\omega\varepsilon)}{d\omega}\right]|\boldsymbol{E}(\boldsymbol{r})|^2 + \mu|\boldsymbol{H}(\boldsymbol{r})|^2\right]\right]}$, where ω is optical frequency, ε is the material permittivity, and $\boldsymbol{E}(\boldsymbol{r})$ and $\boldsymbol{H}(\boldsymbol{r})$ are the electrical field and magnetic field, respectively.

Determining Input Power. The contrast between the absolute power reflected at the Au/air and device interfaces (P_{con}) can be expresses as $P_{con} = R_{Au/air} \times P - (R_{Au/air} \times P_1 + R_{device} \times P_2)$, where P_1 and P_2 are the pump laser powers incident on Au and CdSe, respectively, P ($= P_1 + P_2$) is the total incident pump laser power, and $R_{Au/air}$ and R_{device} are the reflectivity at the Au/air interface and at the device interface, respectively. By substituting $P = P_1 + P_2$ into the expression of P_{con}, we can deduce that $P_2 = \frac{P_{con}}{R_{Au/air} - R_{device}}$. The input power absorbed by CdSe P_{in} can be obtained by $P_{in} = A_{CdSe} \times P_2$, where A_{CdSe} is the absorptance of CdSe nanosquare. When considering the multireflection at the interfaces of air/CdSe/Au three layer structure with an incident angle of θ_1, both R_{device} and A_{CdSe} can be calculated by the interference effects at the interfaces analytically. R_{device} can be calculated by $R_{device} = \left|\frac{r_0 + r_1 e^{2i2\pi/\lambda \tilde{n}_{CdSe} h \cos\theta_2}}{1 + r_0 r_1 e^{2i2\pi/\lambda \tilde{n}_{CdSe} h \cos\theta_2}}\right|^2$. A_{CdSe} can be calculated by $A_{CdSe} = 1 - R_{device} - A_{Au}$, where $A_{Au} = n_{Au}\left|\frac{t_0 t_1 e^{i2\pi/\lambda \tilde{n}_{CdSe} h \cos\theta_2}}{1 + r_0 r_1 e^{2i2\pi/\lambda \tilde{n}_{CdSe} h \cos\theta_2}}\right|^2$ is the absorptance of Au film, $\theta_2 = \sin^{-1}(\sin\theta_1/\tilde{n}_{CdSe})$, r_0 and r_1 are the reflection coefficient at the interface of air/CdSe and CdSe/Au, respectively, t_0 and t_1 are the transmission coefficient at the interface of air/CdSe and CdSe/Au, respectively, and here both r and t have already taken the incident angle θ_1 into consideration. h is the thickness of CdSe nanosquare, $\tilde{n}_{CdSe}$ is the refractive index of CdSe, and n_{Au} is the real part of refractive index of Au.

■ ASSOCIATED CONTENT

Supporting Information

The Supporting Information is available free of charge on the ACS Publications website at DOI: 10.1021/acs.nanolett.8b03890.

TEM, SAED, SEM, and AFM images of CdSe gain material, RMS roughness and permittivity of Au film, mode identification for spontaneous emission spectra, integrated peak collected power, line width narrowing effect, lasing spectra and spatial emission patterns under different pump power, comparison between simulation and experiment mode, simulated near field |E| field distribution with various gain, measurement of the input power in experiment, total absolute absorption power calibration (PDF)

■ AUTHOR INFORMATION

Corresponding Author

*E-mail: renminma@pku.edu.cn.

ORCID

Suo Wang: 0000-0001-5386-9170

Ren-Min Ma: 0000-0003-4199-5772

Notes

The authors declare no competing financial interest.

■ ACKNOWLEDGMENTS

This work was supported by the National Natural Science Foundation of China (Nos. 11574012, 11774014, 61521004), the Youth 1000 Talent Plan Fund.

■ REFERENCES

(1) Bergman, D. J.; Stockman, M. I. *Phys. Rev. Lett.* **2003**, *90* (2), No. 027402.

(2) Berini, P.; De Leon, I. *Nat. Photonics* **2012**, *6*, 16−24.

(3) Ma, R.-M.; Oulton, R. F.; Sorger, V. J.; Zhang, X. *Laser Photon. Rev.* **2013**, *7*, 1−21.

(4) Hill, M. T.; Gather, M. C. *Nat. Photonics* **2014**, *8*, 908−918.

(5) Gwo, S.; Shih, C. K. *Rep. Prog. Phys.* **2016**, *79*, No. 086501.

(6) Wang, D.; Wang, W.; Knudson, M. P.; Schatz, G. C.; Odom, T. W. *Chem. Rev.* **2018**, *118*, 2865−2881.

(7) Hill, M. T.; Oei, Y.-S.; Smalbrugge, B.; Zhu, Y. C.; Vries, T.; Veldhoven, P. J.; Otten, F. W. M.; Eijkemans, T. J.; Turkiewicz, J. P.; Waardt, H.; Geluk, E. J.; Kwon, S.-H.; Lee, Y.-H.; Nötzel, R.; Smit, M. K. *Nat. Photonics* **2007**, *1*, 589−594.

(8) Nezhad, M. P.; Simic, A.; Bondarenko, O.; Slutsky, B.; Mizrahi, A.; Feng, L.; Lomakin, V.; Fainman, Y. *Nat. Photonics* **2010**, *4*, 395−399.

(9) Lu, C.-Y.; Chang, S. W.; Chuang, S. L.; Germann, T. D.; Bimberg, D. *Appl. Phys. Lett.* **2010**, *96*, 251101.

(10) Kim, M. W.; Ku, P.-C. *Appl. Phys. Lett.* **2011**, *98*, 131107.

(11) Ding, K.; Liu, Z. C.; Yin, L. J.; Hill, M. T.; Marell, M. J. H.; van Veldhoven, P. J.; Nöetzel, R.; Ning, C. Z. *Phys. Rev. B: Condens. Matter Mater. Phys.* **2012**, *85*, No. 041301(R).

(12) Ding, K.; Yin, L.; Hill, M. T.; Liu, Z.; van Veldhoven, P. J.; Ning, C. Z. *Appl. Phys. Lett.* **2013**, *102*, No. 041110.

(13) Ding, K.; Hill, M. T.; Liu, Z. C.; Yin, L. J.; van Veldhoven, P. J.; Ning, C. Z. *Opt. Express* **2013**, *21*, 4728−4733.

(14) Gu, Q.; Shane, J.; Vallini, F.; Wingad, B.; Smalley, J. S. T.; Frateschi, N. C.; Fainman, Y. *IEEE J. Quantum Electron.* **2014**, *50*, 499−509.

(15) Pan, S. H.; Gu, Q.; Amili, A. E.; Vallini, F.; Fainman, Y. *Optica* **2016**, *3*, 1260−1265.

(16) Oulton, R. F.; Sorger, V. J.; Zentgraf, T.; Ma, R.-M.; Gladden, C.; Dai, L.; Bartal, G.; Zhang, X. *Nature* **2009**, *461*, 629−632.

(17) Lu, Y.-J.; Kim, J.; Chen, H.-Y.; Wu, C.; Dabidian, N.; Sanders, C. E.; Wang, C.-Y.; Lu, M.-Y.; Li, B.-H.; Qiu, X.; Chang, W.-H.; Chen, L.-J.; Shvets, G.; Shih, C.-K.; Gwo, S. *Science* **2012**, *337*, 450−453.

(18) Liu, X.; Zhang, Q.; Yip, J. N.; Xiong, Q.; Sum, T. C. *Nano Lett.* **2013**, *13*, 5336−5343.

(19) Sidiropoulos, T.; Röder, R.; Geburt, S.; Hess, O.; Maier, S. A.; Ronning, C.; Oulton, R. F. *Nat. Phys.* **2014**, *10*, 870−876.

(20) Zhang, Q.; Li, G.; Liu, X.; Qian, F.; Li, Y.; Chien Sum, T.; Lieber, C. M.; Xiong, Q. *Nat. Commun.* **2014**, *5*, 4953.

(21) Lu, Y.-J.; Wang, C.-Y.; Kim, J.; Chen, H.-Y.; Lu, M.-Y.; Chen, Y.-C.; Chang, W.-H.; Chen, L.-J.; Stockman, M. I.; Shih, C.-K.; Gwo, S. *Nano Lett.* **2014**, *14*, 4381−4388.

(22) Ho, J.; Tatebayashi, J.; Sergent, S.; Fong, C. F.; Iwamoto, S.; Arakawa, Y. *ACS Photonics* **2015**, *2*, 165−171.

(23) Ho, J.; Tatebayashi, J.; Sergent, S.; Fong, C. F.; Ota, Y.; Iwamoto, S.; Arakawa, Y. *Nano Lett.* **2016**, *16*, 2845−2850.

(24) Chou, Y. H.; Wu, Y. M.; Hong, K. B.; Chou, B. T.; Shih, J. H.; Chung, Y. C.; Chen, P. Y.; Lin, T. R.; Lin, C. C.; Lin, S. D.; Lu, T. C. *Nano Lett.* **2016**, *16*, 3179−3186.

(25) Yu, H.; Sidiropoulos, T.; Liu, W.; Ronning, C.; Petrov, P. K.; Oh, S. H.; Maier, S. A.; Jin, P.; Oulton, R. F. *Adv. Opt. Mater.* **2017**, *5*, 1600856.

(26) Lee, C. J.; Yeh, H.; Cheng, F.; Su, P. H.; Her, T. H.; Chen, Y. C.; Wang, C. Y.; Gwo, S.; Bank, S. R.; Shih, C. K.; Chang, W. H. *ACS Photonics* **2017**, *4*, 1431−1439.

DOI: 10.1021/acs.nanolett.8b03890
Nano Lett. 2018, 18, 7942−7948

(27) Kress, S. J. P.; Cui, J.; Rohner, P.; Kim, D. K.; Antolinez, F. V.; Zaininger, K. A.; Jayanti, S. V.; Richner, P.; McPeak, K. M.; Poulikakos, D.; Norris, D. J. *Sci. Adv.* **2017**, *3*, No. e1700688.
(28) Chen, H−Z.; Wang, S.; Ma, R.-M. *IEEE J. Quantum Electron.* **2018**, *54*, 7200307.
(29) Hill, M. T.; Marell, M.; Leong, E. S. P.; Smalbrugge, B.; Zhu, Y.; Sun, M.; van Veldhoven, P. J.; Jan Geluk, E.; Karouta, F.; Oei, Y.-S.; Nötzel, R.; Ning, C.-Z.; Smit, M. K. *Opt. Express* **2009**, *17*, 11107−11112.
(30) Noginov, M. A.; Zhu, G.; Belgrave, A. M.; Bakker, R.; Shalaev, V. M.; Narimanov, E. E.; Stout, S.; Herz, E.; Suteewong, T.; Wiesner, U. *Nature* **2009**, *460*, 1110−1112.
(31) Meng, X. G.; Kildishev, A. V.; Fujita, K.; Tanaka, K.; Shalaev, V. M. *Nano Lett.* **2013**, *13*, 4106−4112.
(32) Zhang, C.; Lu, Y.; Ni, Y.; Li, M.; Mao, L.; Liu, C.; Zhang, D.; Ming, H.; Wang, P. *Nano Lett.* **2015**, *15*, 1382−1387.
(33) Galanzha, E. I.; Weingold, R.; Nedosekin, D. A.; Sarimollaoglu, M.; Nolan, J.; Harrington, W.; Kuchyanov, A. S.; Parkhomenko, R. G.; Watanabe, F.; Nima, Z.; Biris, A. S.; Plekhanov, A. I.; Stockman, M. I.; Zharov, V. P. *Nat. Commun.* **2017**, *8*, 15528.
(34) Yu, K.; Lakhani, A.; Wu, M. C. *Opt. Express* **2010**, *18*, 8790−8799.
(35) Kwon, S. H.; Kang, J.-H.; Seassal, C.; Kim, S. K.; Regreny, P.; Lee, Y. H.; Lieber, C. M.; Park, H. G. *Nano Lett.* **2010**, *10*, 3679−3683.
(36) Ma, R.-M.; Oulton, R. F.; Sorger, V. J.; Bartal, G.; Zhang, X. *Nat. Mater.* **2011**, *10*, 110−113.
(37) Ma, R.-M.; Ota, S.; Li, Y. M.; Yang, S.; Zhang, X. *Nat. Nanotechnol.* **2014**, *9*, 600−604.
(38) Wang, X.-Y.; Wang, Y.-L.; Wang, S.; Li, B.; Zhang, X.-W.; Dai, L.; Ma, R.-M. *Nanophotonics* **2016**, *5*, 52−58.
(39) Guo, C.-C.; Xiao, J.-L.; Yang, Y.-D.; Zhu, Z.-H.; Huang, Y.-Z. *IEEE Photonics Technol. Lett.* **2016**, *28*, 217−220.
(40) Chen, H.-Z.; Hu, J.-Q.; Wang, S.; Li, B.; Wang, X.-Y.; Wang, Y.-L.; Dai, L.; Ma, R.-M. *Sci. Adv.* **2017**, *3*, No. e1601962.
(41) Wang, S.; Li, B.; Wang, X.-Y.; Chen, H.-Z.; Wang, Y.-L.; Zhang, X.-W.; Dai, L.; Ma, R.-M. *ACS Photonics* **2017**, *4*, 1355−1360.
(42) Wang, S.; Wang, X.-Y.; Li, B.; Chen, H.-Z.; Wang, Y.-L.; Dai, L.; Oulton, R. F.; Ma, R.-M. *Nat. Commun.* **2017**, *8*, 1889.
(43) Lakhani, A. M.; Kim, M. K.; Lau, E. K.; Wu, M. C. *Opt. Express* **2011**, *19*, 18237−18245.
(44) Karami Keshmarzi, E.; Tait, R. N.; Berini, P. *Nanoscale* **2018**, *10*, 5914−5922.
(45) Cheng, P.-J.; Huang, Z.-T.; Li, J.-H.; Chou, B.-T.; Chou, Y.-H.; Lo, W.-C.; Chen, K.-P.; Lu, T.-C.; Lin, T.-R. *ACS Photonics* **2018**, *5*, 2638−2644.
(46) Khajavikhan, M.; Simic, A.; Katz, M.; Lee, J. H.; Slutsky, B.; Mizrahi, A.; Lomakin, V.; Fainman, Y. *Nature* **2012**, *482*, 204−207.
(47) Hayenga, W. E.; Gracia, H. G.; Hodaei, H.; Reimer, C.; Morandotti, R.; LiKamWa, P.; Khajavikhan, M. *Optica* **2016**, *3*, 1187−1193.
(48) Ma, R.-M.; Yin, X. B.; Oulton, R. F.; Sorger, V. J.; Zhang, X. *Nano Lett.* **2012**, *12*, 5396−5402.
(49) Chou, Y.-H.; Hong, K.-B.; Chang, C.-T.; Chang, T.-C.; Huang, Z.-T.; Cheng, P.-J.; Yang, J.-H.; Lin, M.-H.; Lin, T.-R.; Chen, K.-P.; Gwo, S.; Lu, T.-C. *Nano Lett.* **2018**, *18*, 747−753.
(50) Shen, K. C.; Ku, C.-T.; Hsieh, C.; Kuo, H.-C.; Cheng, Y.-J.; Tsai, D. P. *Adv. Mater.* **2018**, *30*, 1706918.
(51) Zhou, W.; Dridi, M.; Yong Suh, J.; Hoon Kim, C.; Co, D. T.; Wasielewski, M. R.; Schatz, G. C.; Odom, T. W. *Nat. Nanotechnol.* **2013**, *8*, 506−511.
(52) van Beijnum, F.; van Veldhoven, P. J.; Geluk, E. J.; de Dood, M. J. A.; Hooft, G. W.; van Exter, M. P. *Phys. Rev. Lett.* **2013**, *110*, 206802.
(53) Yang, A.; Hoang, T. B.; Dridi, M.; Deeb, C.; Mikkelsen, M. H.; Schatz, G. C.; Odom, T. W. *Nat. Commun.* **2015**, *6*, 6939.
(54) Schokker, A. H.; Koenderink, A. F. *Optica* **2016**, *3*, 686−693.
(55) Tenner, V. T.; de Dood, M. J. A.; van Exter, M. P. *ACS Photonics* **2016**, *3*, 942−946.
(56) Wang, D.; Yang, A.; Wang, W.; Hua, Y.; Schaller, R. D.; Schatz, G. C.; Odom, T. W. *Nat. Nanotechnol.* **2017**, *12*, 889−894.
(57) Wang, D.; Bourgeois, M. R.; Lee, W.-K.; Li, R.; Trivedi, D.; Knudson, M. P.; Wang, W.; Schatz, G. C.; Odom, T. W. *Nano Lett.* **2018**, *18*, 4549−4555.
(58) Stratton, J. A.; Chu, L. J. *Phys. Rev.* **1939**, *56*, 99−107.

DOI: 10.1021/acs.nanolett.8b03890
Nano Lett. 2018, 18, 7942−7948